Quest: Journal of Geometry, Mathematical and Quantum Physics
e-ISSN: 3064-7282 Vol.3 Issue 2|2026

Improving the Performance of the P-Cui/N-Inse Photodetector by Adding Back-Reflective and Interlayer Layers Using SCAPS-1D

Naeemah A. Aswad, Assist. Prof. Dr. Ayed N. Saleh
Department of Physics, College of Education for pure science, University of Tikrit, Iraq

Abstract: The p-cui/n-InSe photodetector was studied using the SCAPS-1D simulation program. We improved the detector by changing the thickness of some layers and introducing back-reflecting layers (BSL) onto the basic detector until we obtained the highest specific detection value, which was $8.29*10^{13}$cm.$HZ^{1/2}W^{-1}$. Then, we added interlayers with a thickness of 0.03 mW until we obtained the highest specific detection value, which was $9.30*10^{13}$cm$HZ^{1/2}W^{-1}$. Then, the best back-reflecting layer, which was InP, was combined with the best interlayer, which was PEDOT: PSS, and placed between the p-cui layer and the n-InSe absorption layer. Thus, we obtained an improved detector with a specific detection value of $2.57*10^{15}$cm.$HZ^{1/2}$ W^{-1}.

Keywords: p–CuI/n–InSe heterojunction . SCAPS-1D simulation. photodetector. optoelectronic properties.

Introduction

Photodetector technology in general, and near-infrared detectors in particular, are considered among the most important industrial technologies today due to their significance in a wide range of applications, such as gas sensors, spectroscopy, and night vision. A photodetector is defined as a device used to detect light radiation by absorbing incident photons. It converts light energy into electrical signals in the form of current and voltage. Sometimes it is called a photosensitive device, and the principle behind this process is known as photo detection [1]. For several decades, researchers have focused on using compounds such as InAs, Insb, and CdTe in the manufacture of thin films for electronic devices such as photodetectors and solar cells. This is due to the high efficiency of these materials. However, their high cost, large footprint, scarcity of some, and toxicity of others have led researchers to seek alternatives. Therefore, researchers have sought to replace them with other readily available, non-toxic materials with good electrical and optical properties. One such material is the chalcogenide InSe, which is a good candidate due to its availability, low cost, and direct energy gap. With an energy of 1.25eV, close to the ideal value, interest in these materials and the study of their optical and electrical properties has increased. Indium selenide is a semiconductor material belonging to Group III-VI, and in its natural state, it is of the n-type [2]. This compound has been used in near-infrared detection, as infrared radiation is part of the electromagnetic spectrum with wavelengths ranging from 0.7 µm to 30 µm. Infrared detectors are used to convert light signals into electrical signals. Equation (1) illustrates the relationship between the photon energy E, the wavelength m, and the frequency f [3].

$$E=hf=\frac{hc}{\lambda} \quad \text{.................................}(1)$$

Infrared radiation has been divided into five regions as shown in Table (1).

Table 1. Infraed Wavelengh regions [3].

μm	Name
0.7-1	Near Infrare(NIR)
1-3	Sort-wave Infrared (SWIR)
3-5	Mid-Wave Infrered (MWIR)
8-12	Long-wave Infrared(LWIR)
12-30	Very-long wave Infrared(VLWIR)

In our current study, near-infrared radiation was detected using the absorption layer of the InSe photodetector. The experimental results were compared with the simulation results, and the possibility of improving the photodetector's properties was explored by adding a reflective layer and an interlayer, and by adding substitution elements to the InSe composite to improve the photodetector's efficiency.

Simulation Method

SCAPS-1D is a one-dimensional device simulation program developed in the Department of Electronics and Information Systems (ELIS) at the University of Ghent [4-5] in Belgium. The program uses one-dimensional simulation of conventional semiconductor crystalline materials for p-cui/n-InSe photodetector layers. It allows the user to describe photodetector properties such as optical absorption, thickness, doping concentration, energy gap, and other characteristics. Various detector parameters are defined, including quantitative efficiency, spectral response, qualitative detection, and the magnitude of the current-voltage curve change, which are calculated when the detector is exposed to light and in darkness. SCAPS-1D is a free program that relies on solving a set of equations, including Poisson's equation [6].

$$\nabla(E) = \frac{q}{\varepsilon}(p - n + N_D^+ - N_A^-) \quad (2)$$

Where q is the electron charge, E is the electric field, n is the electron density, p is the hole density, N_D is the electron donor concentration, N_A is the electron acceptor concentration, and d is the absorption permittivity.

The continuity equation is given by the following relation [7].

$$\frac{d_n}{d_t} = \frac{1}{q}(\nabla(J_n) + G_n - R_n \quad (3)$$

$$\frac{d_p}{dt} = -\frac{1}{q}(\nabla(J_P) + G_p - R_P \quad (4)$$

Where G_n is the electron generation rate, G_P is the hole generation rate, J_n is the electron current density, J_P is the hole current density, R_n is the electron recombination rate, and R_p represents the hole recombination rate.

The charge carrier equations for diffusion and drift currents are calculated according to the following equations:[8]

$$J_n = q(\mu_n nE + D_n \nabla_n) \quad (5)$$

$$J_p = q(\mu_n PE + D_P \nabla_P) \quad (6)$$

Where D is the diffusion constant and μ_n and p_μ are the electron mobility and hole mobility.

The device structure was defined by the properties of suitable materials, their thickness and dimensions, and then the main parameters such as bias voltage, incident light wavelength, required frequency and intensity were determined according to the simulation requirements. The simulation was conducted under specific conditions of temperature (300K) and hypothetical illumination conditions (1000 mW/cm² = 1000 W/m²) with a global air mass of 1.5 [9]. To measure the performance of the photodetector, it is necessary to study its parameters, namely quantitative efficiency, spectral response, specific detection, and current-voltage relationship.

These parameters are interconnected and related to equations 5 and 6. The spectral response, R, is defined as the ratio of the photocurrent (I_{Ph}) generated by the photodetector to the incident luminous power (P_{opt}) at a specific wavelength (m), and is expressed in units of A/W (amperes per watt). The photoresponse was then calculated using the following formula [10]:

$$\mathcal{R} = \frac{I_{ph}}{P_0} \quad Or \quad \mathcal{R} = \frac{V_{ph}}{P_0} \quad (7)$$

Where I_{ph} is the optical current, and P_0 is the incident optical power. Quantum efficiency is defined as the ratio of the number of electrons collected at the detector terminals to the number of incident photons. Quantum efficiency is expressed as a percentage and is calculated using the following equation [11]:

$$\eta = \frac{N_{carriers}}{N_{photons}} = \frac{(I_{ph}/q)}{(P_s/hv)} \quad (8)$$

Where I_{ph} is the optical current, q is the charge, h is Planck's constant, v is the frequency, and P_S is the optical power.

Specific detection (D*) is a term used to compare different types of photodetectors. Specific detection is measured in $cm/Hz^{1/2}\ W^{-1}$ and is defined by the following relationship [11]:

$$D^* = \frac{(A.\Delta f)^{1/2}}{NEP} = (A.\Delta f)^{1/2}.D \quad (9)$$

Where A is the area of the photodetector, Δf is the frequency bandwidth and D is the detection range.

Device Structure

The photodetector in its simplest form p-cui/n-InSe (Figure 1) consists of two layers: the p-cui transmitting layer, a semiconductor material with a relatively wide energy gap and a suitable thickness of 0.06μm and a concentration of $8*10^{18}cm^{-3}$, followed by the n-InSe absorbing layer, which has a small energy gap and a thickness of 0.8μm and a concentration of $3*10^{15}cm^{-3}$, according to Table (2), which shows the program parameter values at room temperature 300k and at a reverse bias voltage of (-0.5)V.

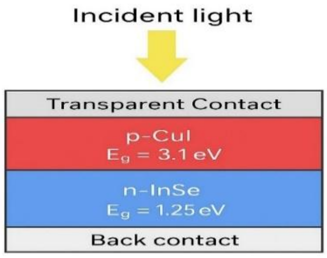

Fig 1. Shows Device Structure.

Table 2. shows the most important basic detector parameters in the SCAPS simulation program.

Layers	Eg(eV)	μn(cm^2/v.s)	P(cm^2/v.s)μ	Ne(cm^{-3})	Nv(cm^{-3})	Electron affinityχ(eV)	Donor density (cm^{-3})	Accept density (cm^{-3}
p-cui [12]	3.1	100	50	$2.8*10^{19}$	$1*10^{19}$	2.1	$8*10^{18}$	$1*10^{1}$
InSe [13]	1.25	1000	100	$1.57*10^{18}$	$3.63*10^{19}$	4.7	$3*10^{15}$	0

Simulation Parameters

The simulation was conducted at 300 K with AM1.5G solar spectrum illumination (100 mW/cm^2). The applied voltage ranged from -0.8 V to 0 V, and it was assumed that the front and rear contacts were both Ohmic. Defect densities, carrier mobilities, electron affinity (χ), and bandgap energy

(E_g) were among the components of the model that were borrowed from earlier theoretical and experimental investigations [3-5]. Table (1) displays the key photodetector parameters utilized in the p-CuI/n-InSe simulation.

Table 1. presents the principal fundamental detector settings inside the SCAPS simulation software.

Layers	E_g (eV)	μ_n (cm^2/v.s)	μ_P (cm^2/v.s)	Nc (cm^{-3})	Nv (cm^3)	Electron affinityχ(V)
p-CuI [5]	3.1	100	50	$2.8*10^{19}$	$1*10^{19}$	2.1
InSe [3]	1.25	1000	100	$1.57*10^{18}$	$3.63*10^{19}$	4.7

Results and discussion

In the current study, a p-cui/n-InSe type photodetector is discussed and simulated. When the p-cui transducer layer is exposed to light at room temperature 300k and a reverse bias voltage of -0.5V is applied, the characteristics of the photodetector in its simplified form are studied. Then, different back-reflective layers (BSL) and interlayers are added to improve the best performance of the photodetector. The best reflective layer and the best interlayer are then selected, and the effect of this on the photodetector parameters is studied. The final stage involves changing the energy gap by adding elements in certain proportions to the InSe absorption layer to broaden the spectral region.

Simulation of the p-cui/n-InSe photodetector in its ideal state

The 0.80µm thick InSe absorption layer has an energy gap of 1.25eV and operates at a voltage range of -0.7V to 0V. When the program is run in the dark, we observe, as shown in Figure (2-a) of the (I-V) curve characteristics, very low values of dark current, which equal $2.03*10^{-10}$ mA/cm^2 at a reverse bias voltage of -0.5V, resulting from the thermal energy of the minority carriers. Figure (2-b) shows the quantum efficiency as a function of wavelength, which starts at a wavelength of 200nm and then gradually increases until it reaches its highest value at near-infrared wavelengths, and then begins to decrease at a wavelength of 980nm. This is consistent with the behavior of the photodetector with an n-InSe absorption layer and an energy gap of 1.25eV [14]. Figure (2-c) shows the spectral response and Figure (2-d) shows the specific detection as a function of wavelength, which begins to decrease when approaching the absorption edge because the photon energy becomes less than the energy gap of the InSe material [15]. Thus, InSe-based photodetectors show a wide-range response from visible wavelengths to near-infrared wavelengths, and this is consistent with the researcher's practical study [16].

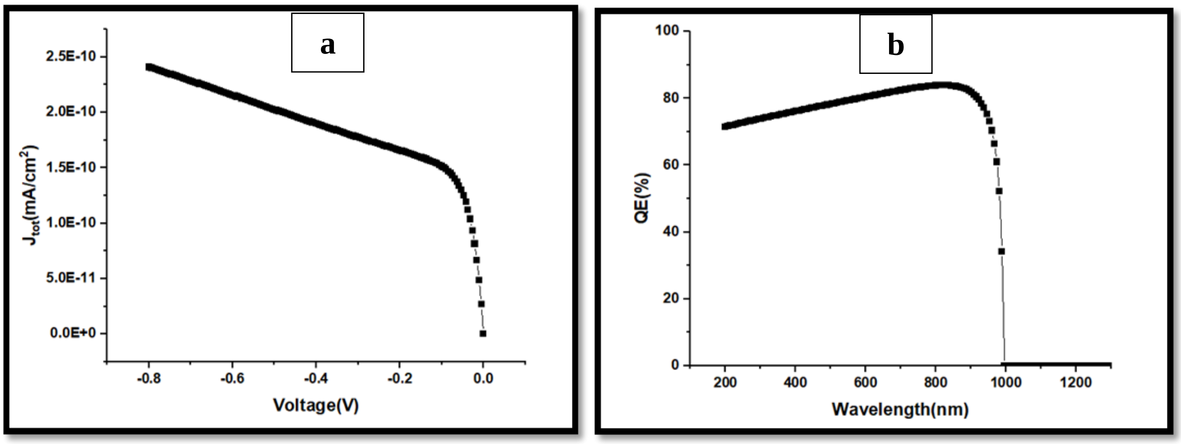

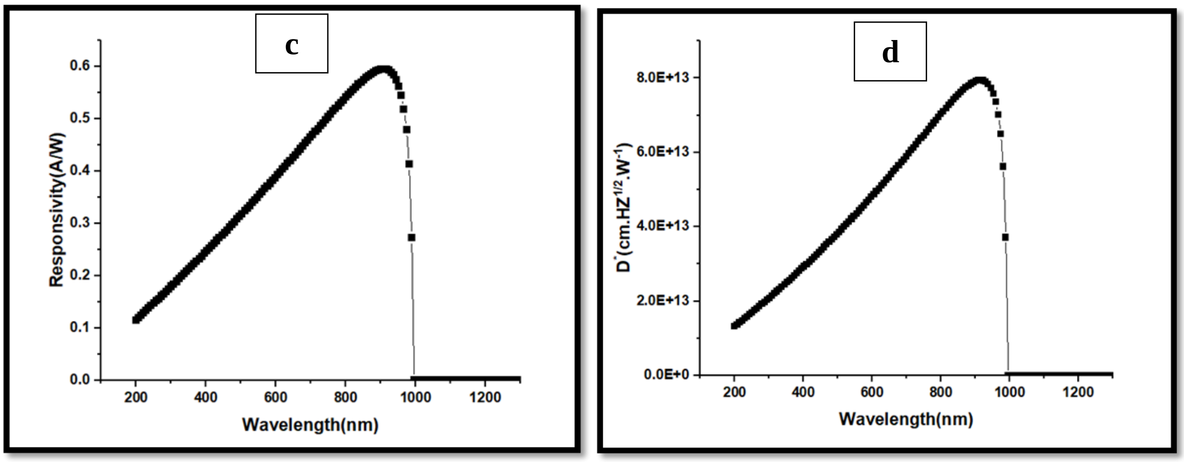

Fig 2. Shows (a)- Current-voltage characteristic curves of the p-cui/n-ins photodetector (b)- Quantum efficiency as a function of wavelength (c)- Spectral response as a function of wavelength (d)- Spectral detectability as a function of wavelength.

Table 3. Key parameters of the p-cui/n-InSe photodetector.

model	**IDmA/cm^2**	**QE%**	**Responsivity(A/W)**	**D*(cm.HZ$^{1/2}$.W^{-1})**
p-cui/ n-InSe	$2.03*10^{-10}$	83.89	0.595	$7.94*10^{13}$

Simulating the effect of a background reflection layer

To improve the p-cui/n-InSe photodetector, we study the effect of adding different backscatter layers (BSL), which consist of the following compounds: (ZnSe-TiO_2-Azo-Inp-GaAs), which are of the n type, and whose properties are shown in Table (4). The benefit of the backscatter layer (BSL) is primarily to reflect the photons passing from the absorption layer, and this leads to an increase in the concentration of carriers and reduces the recombination process [17].

Table 4. Basic parameters of the BSL (Back Reflection Layer).

Parameter	**Symbol (unit)**	**ZnSe[18,19]**	**TiO_2[20]**	**AZO[21]**	**Inp[22]**	**GaAS [23, 24]**
Thickness	d(μm)	0.05	0.03	0.03	0.03	0.05
Band gap	Eg (eV)	2.8	3.2	3.3	1.34	1.42
Electron affinity	χ(eV)	4.09	4.5	4.5	4.3	4.07
Dielectric permittivity	r**ε**/**ε**	9	10	9	12.5	12.9
CBeffective density of states	Nc(cm^{-3})	$4*10^{18}$	$1*10^{21}$	$4*10^{18}$	$1*10^{17}$	$4.35*10^{17}$
VB effective density of states	N_v(cm^{-3})	$1*10^{18}$	$1*10^{19}$	$9*10^{18}$	$1*10^{19}$	$1.29 *10^{19}$
Electron thermal velocity	V_n(cm/s)	$1*10^7$	$1*10^7$	$1*10^7$	$1*10^7$	$1*10^7$
Hole thermal velocity	V_p(cm/s)	$1*10^7$	$1*10^7$	$1*10^7$	$1*10^7$	$1*10^7$
Electron mobility	μ_n(cm^2/v.s)	530	1*10-3	1*102	55*102	$88*10^2$
Hole	μp(cm2/v.s)	28	$1*10^{-2}$	$2.5*10^1$	$3*10^2$	$4*10^2$

mobility						
Donor density	N_D (cm^{-3})	$1*10^{17}$	$1*10^{19}$	$1*10^{20}$	$1*10^{18}$	$1*10^{16}$
Acceptor density	N_A(cm^{-3})	0	0	0	0	0

Important parameters that determine the conduction band shift are electron affinity and the energy gap. The basic equation that can be used to determine the conduction band shift is as follows:

$CBO= \nabla E_c = \chi_{\text{Absorbers}} - \chi_{\text{Reflection}}$ (10)

Where ∇E_c represents the electron affinity difference between the two conduction bands, $\Delta \chi_{\text{Absorbers}}$ is the electron affinity of the absorbing layer, and $\Delta \chi_{\text{Reflection}}$ is the electron affinity of the reflecting layer.

The valence band shift equation is determined by the following relationship:

$VBO = \nabla E_v = [\chi_{\text{Absorber}} + E_{g(\text{Absorber})}] - [\chi_{\text{Reflection}} + E_{g(\text{Reftection})}]$ (11)

Where ∇E_v represents the electron affinity difference between the two valence bands, $E_{g(\text{Absorber})}$ is the energy gap of the absorption layer, and $E_{g(\text{Reflection})}$ is the energy gap of the reflection layer. Figure (3-a) shows the effect of adding BSL layers by comparing them to the photodetector before the addition. This had a significant impact on the current-voltage characteristic curve. Regarding the quantum efficiency, spectral response, and specific detection curves as a function of wavelength and at a reverse bias voltage (-0.5V), as shown in Figures (3-b), (3-c), and (3-d), which illustrate the photodetector parameters, an increase in the quantum efficiency, spectral response, and specific detection is observed when compared to the photodetector before the addition of the back reflection layers. A clear improvement is also observed in the specific detection curve, especially for the Inp and GaAS back reflection layers, thus making it superior. The two reflection layers are (Inp and GaAS layer). This is due to the displacement of the conduction band between the reflection layer and the absorption layer. This prevents recombination and increases the efficiency of the photodetector [25]. Although the highest specific detection was obtained with the GaAS back reflection layer, the Inp layer was considered the best reflection layer because of its compatibility with the other detector layers and its ability to give the best results later on.

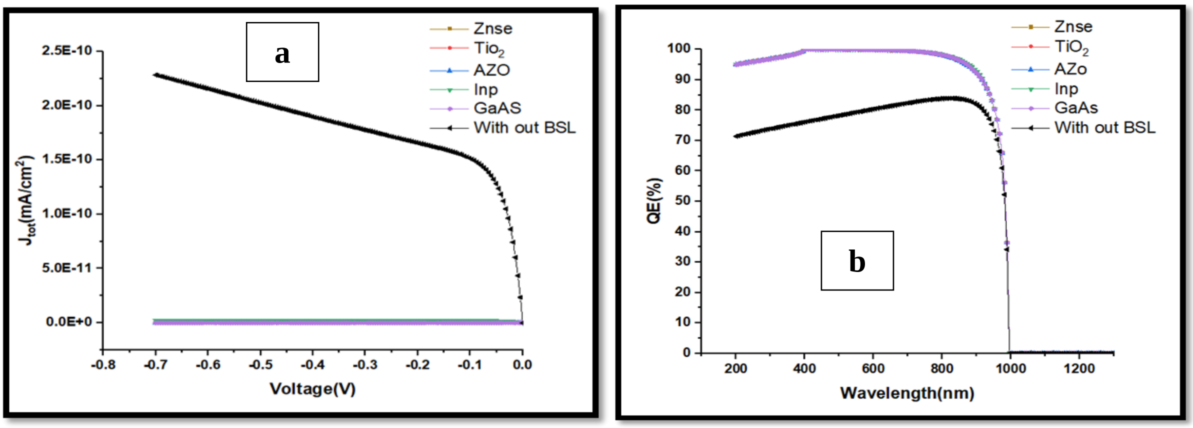

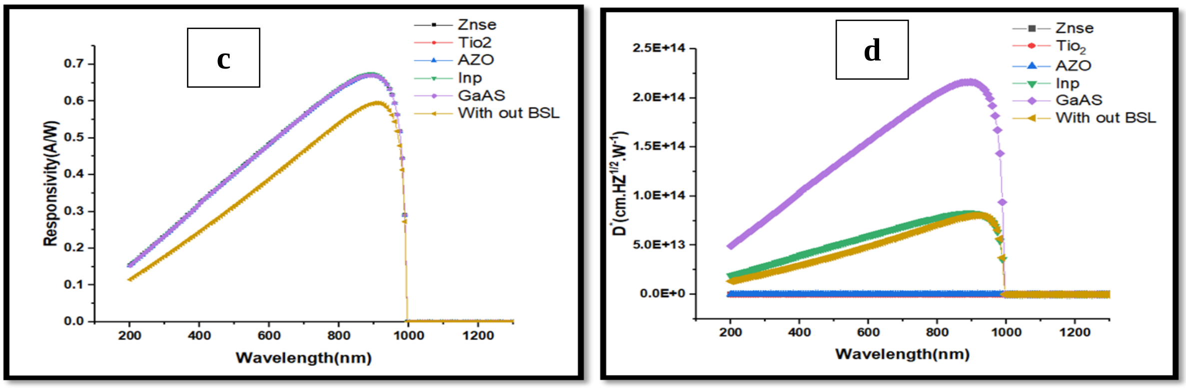

Fig 3. Shows (a)- The curve illustrates the inverse current-voltage (I-V) characteristic after the addition of a BSL layer. (b)- Quantum efficiency as a function of wavelength and, upon the addition of BSL back-reflective layers (c)- Spectral response as a function of wavelength and, upon the addition of BSL back-reflective layers (d)-Spectral detectance as a function of wavelength upon the addition of a BSL layer.

Table (5) shows the output results of the photodetector after adding the back reflection layers.

Table 5. Photodetector outputs after adding the reflective layer.

Material	J_{tot}(mA/cm^2)	QE(%)	Responsivity(A/W)	Qualitative detection(cm.HZ$^{1/2}$.W^{-1})
Znse	$3.025*10^{-45}$	99.38	0.65	0
TiO_2	$3.003*10^{-15}$	99.38	0.65	0
AZO	$3.02*10^{-45}$	99.38	0.65	0
Inp	$2.07*10^{-12}$	99.53	0.66	$8.29*10^{13}$
GaAS	$3.00*10^{-15}$	99.47	0.65	$2.16*10^{14}$
Without BSL	$2.06*10^{-10}$	82.50	0.57	$7.9*10^{13}$

From the above, and through the results in Table (5), it is clear that the best reflective layer is the Inp layer, as the back reflection layer led to the generation of a high electron potential barrier, which in turn led to a greater reflection process, and consequently, a significant improvement in the parameters of the photodetector [25]. Thus, the photodetector, after selecting the best reflective layer, becomes as shown in Figure (4):

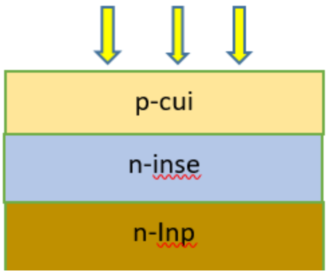

Fig 4. The photodetector after adding the reflective layer.

Simulating the effect of the interlayer

After selecting the best reflective layer, the Inp layer, and adding it to the original detector layers in this study, the best buffer layer placed between the Cui transmitting layer and the InSe absorbing layer will be tested, and its effect on the photodetector parameters will be studied. Several p-type buffer layers were added to the detector after optimization, while maintaining the stability of all photodetector parameters. These layers are (Pss, Cu_2O, CuO, CZTSSe, CUSbs3), which are characterized by having the lowest absorption loss and the ability to output photocurrent carriers created with minimal recombination losses, then transfer them to the external circuit. They also have a suitable energy gap to allow the passage of the maximum possible number of carriers to the absorbing layer. The main role of this layer is to form an interface with the absorbing layer and conduct the maximum number of photons [26].

Table (6) shows the most important parameters of the buffer layers.

Table 6. Basic parameters of p-type buffer layers.

Parameters	**Symbol(unit)**	**PEDOT:Pss[27]**	**Cu_2O[28]**	**CuO[29]**	**CZTSSe[30]**	**$Cusbs_3$[31]**
Thickness	W(μm)	0.03	0.02	0.03	0.03	0.03
Bandgap	Eg(eV)	2.2	2.2	2.1	1.3	1.5
Electron affinity	χ(eV)	2.9	3	3.2	4.1	4.2
Dielectric Permittivity	εr	3	7.5	7.11	13.6	10
CB effective density of states	Nc(cm^{-3})	$2.2*10^{15}$	$2*10^{19}$	$2.2*10^{20}$	$2.20*10^{18}$	$2.2*10^{18}$
VB effective density of states	Vv(cm^{-3})	$1.8*10^{19}$	$1*10^{19}$	$5.5*10^{19}$	$1.8*10^{19}$	$1.8*10^{19}$
Electron thermal velocity	Vn(cm/s)	$1.000*10^{+7}$	$1.00*10^{+7}$	$1.000*10^{+7}$	$1.00*10^{+7}$	$1.00*10^{+7}$
Hole thermal velocity	Vp(cm/s)	$1.000*10^{+7}$	$1.000*10^{+7}$	$1.000*10^{+7}$	$1.00*10^{+7}$	$1.00*10^{+7}$
Electron mobility	μ_n(cm^2/v.s)	$2*10^{-2}$	200	3.4	$1*10^2$	$1.00*10^2$
Hole mobility	μ_p(cm^2/v.s)	$2*10^{-4}$	8600	3.4	$2.5*10^1$	$2.500*10^{+1}$
Donor density	ND($1/cm^3$)	0	0	0	0	0
Acceptor density	NA($1/cm^3$)	$1*10^{18}$	$1*10^{18}$	$1*10^{18}$	$1*10^{19}$	$1.000*10^{20}$
Coefficient absorption	α(1/cm)	$1*10^{+5}$	-	$1*10^{+5}$	-	-

When studying the p-cui/n-InSe photodetector with the addition of several interlayers in order to obtain the best photodetector tool, an improvement in the detector parameters was noted. When using the PEDOT:PSS layer, which has an energy gap of 2.2eV, which gave the best results, the PEDOT:PSS layer with the original P-CUI detector layer was formed as a double buffer layer, which improved the interface with the n-InSe absorption layer. This layer had higher current carriers in the short wavelength region of 400nm to the long wavelengths corresponding to near-infrared radiation due to its 2.2eV energy gap, which allows for maximum absorption of photons by the absorption layer, which had an effect on improving the photodetector parameters [32].

Figure (5-b) shows the quantitative efficiency, Figure (5-c) the spectral response, and Figure (5-d) the qualitative detectivity as a function of wavelength when adding the PEDOT:PSS layer and at the reverse bias voltage (-0.5V). The figures show a clear improvement in the photodetector parameters compared to the original p-cui/n-InSe photodetector, as the detector has a wide spectral response ranging from 200 nm to 1000 nm. Thus, we can conclude that the additional double buffer layers are transparent for wavelengths greater than 200 nm, and this helps to absorb the greatest number of photons that reach the absorption layer [33].

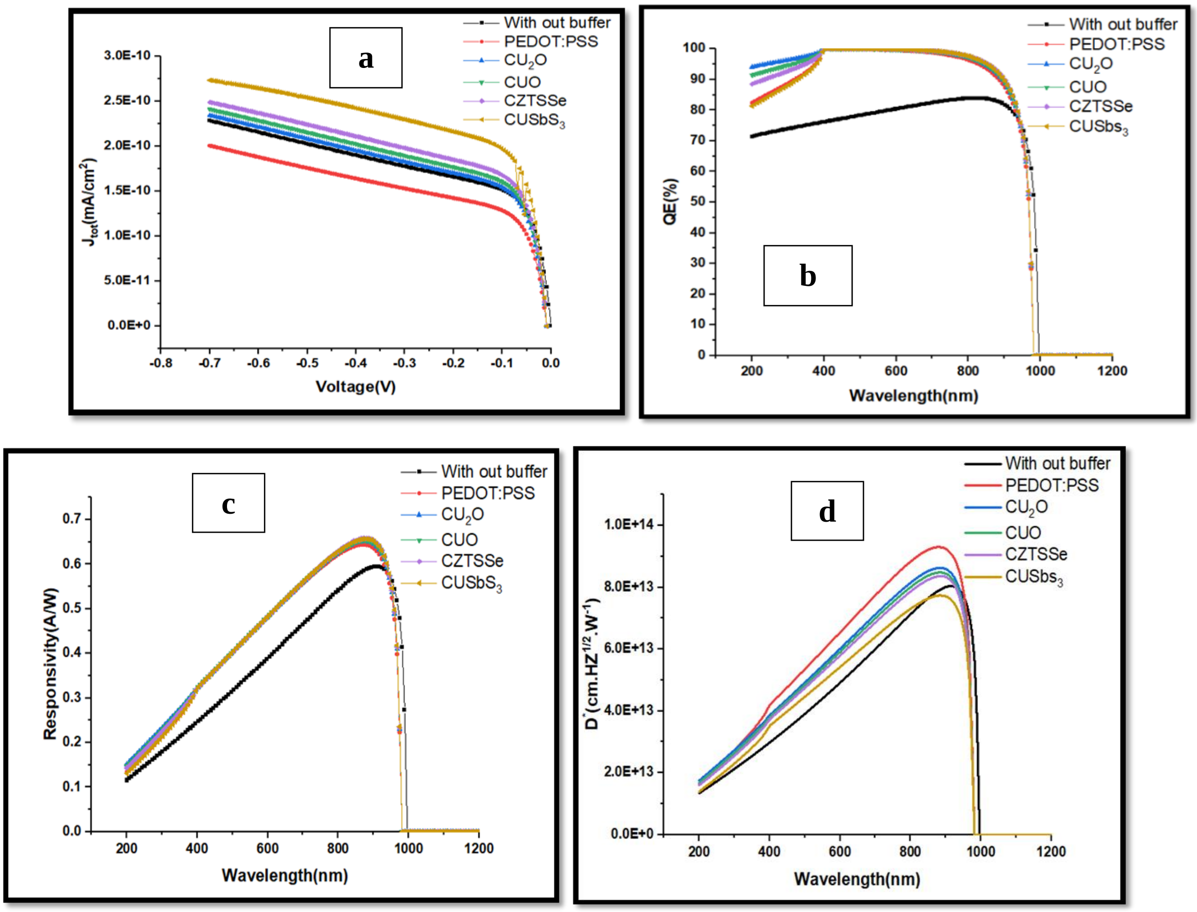

Fig 5. Shows (a)- Current-voltage characteristic curves as the interfacing layers change (b)- Quantum efficiency as a function of wavelength with interfacing layer change (c)- Spectral response as a function of wavelength with interfacing layer change (d)- Spectral detection curve as a function of wavelength with interfacing layer change.

Table (7) shows the output values of the photodetector and the effect of the buffer layer on its operation and performance. It is observed that by changing the PEDOT:PSS buffer layer, we obtained the lowest value for the dark current. Therefore, reducing the dark current of the photodetector can achieve a high detection rate and low noise current.

Table 7. represents the photodetector output after adding buffer layers.

Material	Jtot(mA/cm^2)	QE(%)	Responsivity(A/W)	Qualitative detection(cm.HZ$^{1/2}$.W^{-1})
Without buffer	2.085E-10	82.50	0.588	7.90E13
PEDOT:PSS	1.7706E-10	99.67	0.643	9.30E13
CU2O	2.0916E-10	99.032	0.651	8.63E13
CUO	2.16E-10	99.07	0.652	8.84E13
CZTSSe	2.25E-10	99.25	0.658	8.36E13
CUSbs3	2.55E-10	99.29	0.656	7.73E13

Study and simulation of the best reflective layers and interlayer for the photodetector

After simulating and studying the addition of back reflection layers and the addition of different interlayers at a reverse bias voltage (-0.5V) and a temperature of (300K), we note that the photodetector with the following configuration (P-cui/ P-PEDOT:Pss/ n-InSe/n-Inp) as shown in Figure (6) gave the best results for the photodetector parameters compared to the original p-cui/n-InSe photodetector. Table (8) shows the outputs of the photodetector after adding the two reflection layers n-Inp and the P-PEDOT:PSS interlayer, as we note a clear improvement in all the photodetector parameters.

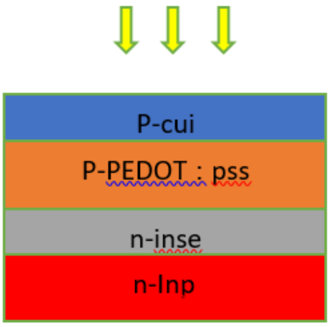

Fig 6. The selected photodetector after adding the reflective layer and the interlayer.

Table 8. Photodetector outputs after adding the reflective layer and interlayers

Material	Jtot(mA/cm^2)	QE(%)	Responsivity(A/W)	Qualitative detection(cm.HZ$^{1/2}$.W^{-1})
P-cui/ P-PEDOT:Pss/ n-InSe/n-Inp	2.12*10^{-13}	99.8	0.67	2.57*10^{15}

Conclusions

A p-cui/n-InSe photodetector was simulated by SCAPS software and then the detector was improved by adding BSL back reflection layers, which resulted in an increase in both the detector's specific detection and spectral response. The reflection layer reduced recombination on the back surface. An interlayer was added, placed between the transmitting layer and the absorbing layer, which led to an increase in the specific detection process, as it allowed photons to pass to the absorbing layer. The best reflection layer with the best interlayer was then selected to achieve an improvement in the detector's characteristics.

Acknowledgements Authors are grateful to the management of the University of Tikrit for their support and encouragement during this work.

Funding No funding was received to assist with the preparation of this manuscript.

Author contribution All authors have contributed equally to the work. All authors have read and agreed to the published version of the manuscript.

Data availability Data will be made available on request. Conflict of interest The authors declare no conflict of interest.

References

1. Capper, Peter, Arthur Willoughby, and Safa O. Kasap. Optical properties of materials and their applications. John Wiley & Sons, 2020.
2. Guo, Yuzheng, and John Robertson. "Band structure, band offsets, substitutional doping, and Schottky barriers of bulk and monolayer InSe." Physical Review Materials 1.4 (2017): 044004.
3. Hobbs, Matthew. Infrared Detectors for Radiation Thermometry. Diss. University of Sheffield, 2014.
4. Decock, Koen, Samira Khelifi, and Marc Burgelman. "Modelling multivalent defects in thin film solar cells." Thin Solid Films 519.21 (2011): 7481-7484.

5. Burgelman, Marc, and Jonas Marlein. "Analysis of graded band gap solar cells with SCAPS." Proceedings of the 23rd European Photovoltaic Solar Energy Conference, Valencia. Citeseer, 2008.
6. Skhouni, Othmane, et al. "Numerical study of the influence of ZnTe thickness on CdS/ZnTe solar cell performance." The European Physical Journal Applied Physics 74.2 (2016): 24602.
7. Hameed, K. Yousaf, et al. "Modelling of novel-structured copper barium tin sulphide thin film solar cells." Bulletin of Materials Science 42.5 (2019): 231.
8. Ganvir, Rasika. "Modelling of the nanowire CdS-CdTe device design for enhanced quantum efficiency in Window-absorber type solar cells." (2016).
9. Burgelman, Marc, and Jonas Marlein. "Analysis of graded band gap solar cells with SCAPS." Proceedings of the 23rd European Photovoltaic Solar Energy Conference, Valencia. 2008.
10. Kasap, Safa O. Optoelectronics and photonics. Vol. 218. Pearson Education UK, 2013.
11. Rogalski, Antoni, Zbigniew Bielecki, and Janusz Mikolajczyk. "Detection of optical radiation." Handbook of optoelectronics. CRC Press, 2017. 65-124.
12. Liu, Jingyu, et al. "Piezo-phototronic effect enhanced UV photodetector based on Cul/ZnO double-shell grown on flexible copper microwire." Nanoscale research letters 11 (2016): 1-7.
13. Yildiz, Elif Akhuseyin. "Single crystalline Holmium doped InSe for optical limiting operation in Near-IR region." Physica Scripta 99.9 (2024): 095941.
14. Kasap, Safa O. Optoelectronics and photonics. Vol. 218. Pearson Education UK, 2013.
15. Rogalski, Antoni, Zbigniew Bielecki, and Janusz Mikolajczyk. "Detection of optical radiation." Handbook of optoelectronics. CRC Press, 2017. 65-124.
16. Luo, Wengang, et al. "Gate tuning of high-performance InSe-based photodetectors using graphene electrodes." Advanced Optical Materials 3.10 (2015): 1418-1423.
17. Guo, Yuzheng, and John Robertson. "Band structure, band offsets, substitutional doping, and Schottky barriers of bulk and monolayer InSe." Physical Review Materials 1.4 (2017): 044004.
18. Feng, Wei, et al. "Ultrahigh photo-responsivity and detectivity in multilayer InSe nanosheets phototransistors with broadband response." Journal of Materials Chemistry C 3.27 (2015): 7022-7028.
19. Bücheler, Stephan Friedrich. Investigation of compound semiconductors as buffer-layer in thin film solar cells. Diss. ETH Zurich, 2010.
20. Sharma, Y., et al. "Bandgap tuning of optical and electrical properties of zinc selenide." Chalcogenide Lett 18 (2021): 183-189.
21. Bahador,AliReza, Mehdi Molaei, and Masoud Karimipour. "Synthesis and characterization of transition metal doped ZnSe/ZnS nanocrystals by a rapid photochemical method." Journal of Nanostructures 9.1 (2019):124130
22. Sawicka-Chudy, P., et al. "Simulation of TiO2/CuO solar cells with SCAPS-1D software." Materials Research Express 6.8 (2019): 085918.
23. Bao, Chunxiong, et al. "Low-noise and large-linear-dynamic-range photodetectors based on hybrid-perovskite thin-single-crystals." Advanced materials 29.39 (2017): 1703209.
24. Zhu, Min, et al. "Simulation and optimization of pin In0. 53Ga0. 47As/InP photodetector." AOPC 2015: Optical and Optoelectronic Sensing and Imaging Technology. Vol. 9674. SPIE, 2015.

25. Djaafar, F., B. Hadri, and G. Bachir. "The Effect of a Back Surface Field (BSF) on the Efficiency of a Dual Junction InGaP/GaAs Cell." The International Conference on Recent Advances in Electrical Systems. 2017.
26. Attari, Kamal, et al. "The design and optimization of GaAs single solar cells using the genetic algorithm and Silvaco ATLAS." International Journal of Photoenergy 2017.1 (2017): 8269358.
27. Baig, Faisal. Numerical analysis for efficiency enhancement of thin film solar cells. Diss. Universitat Politècnica de València, 2019.
28. Eisele, W., et al. "XPS, TEM and NRA investigations of Zn (Se, OH)/Zn (OH) 2 films on Cu (In, Ga)(S, Se) 2 substrates for highly efficient solar cells." Solar energy materials and solar cells 75.1-2 (2003): 17-26.
29. Li, Zhen-Qi, Ming Ni, and Xiao-Dong Feng. "Simulation of the Sb2Se3 solar cell with a hole transport layer." Materials Research Express 7.1 (2020): 016416.
30. Rahman, Naimur, et al. "Assessing the performance of MoTe2 based solar cell with Cu2O hole transport layer through device simulation." Discover Materials 3.1 (2023): 25
31. Ganvir, Rasika. "Modelling of the nanowire CdS-CdTe device design for enhanced quantum efficiency in Window-absorber type solar cells." (2016).
32. Cherouana, Abdelbaki, and Rebiha Labbani. "Study of CZTS and CZTSSe solar cells for buffer layers selection." Applied surface science 424 (2017): 251-255.
33. Olopade, Muteeu, et al. "The study of some materials as buffer layer in copper antimony sulphide (CuSbS 2) solar cell using SCAPS 1-D." 2017 IEEE 44th photovoltaic specialist conference (PVSC). IEEE, 2017.
34. Najim, Alaa H., and Ayed N. Saleh. "Study effect of window and BSF layers on the properties of the CZTS/CZTSe solar cell by SCAPS–1D." Tikrit Journal of Pure Science 24.3 (2019): 77-83.
35. Gao, Zhongliang, et al. "Improving light absorption of active layer by adjusting PEDOT: PSS film for high efficiency Si-based hybrid solar cells." Solar Energy 228 (2021): 299-307.